Chem Biol Drug Des 2007; **69:** 5–13

Research Article

doi: 10.1111/j.1747-0285.2007.00464.x

Binding Pathways of Ligands to HIV-1 Protease: Coarse-grained and Atomistic Simulations

Chia-En A. Chang[1,2,3,*], Joanna Trylska[4], Valentina Tozzini[5] and J. Andrew McCammon[1,2,3,6]

[1]Department of Chemistry and Biochemistry, [2]Center for Theoretical Biological Physics, [3]Howard Hughes Medical Institute, University of California at San Diego, La Jolla, California 92093, USA
[4]Interdisciplinary Centre for Mathematical and Computational Modelling, Warsaw University, 02-106 Warsaw, Poland
[5]NEST-INFM-CNR Scuola Normale Superiore, Piazza dei Cavalieri, 7 I-56126 Pisa, Italy
[6]Department of Pharmacology, University of California at San Diego, La Jolla, California 92093, USA
**Corresponding author: Chia-En A. Chang, cchang@mccammon.ucsd.edu*

Multiscale simulations (coarse-grained Brownian dynamics simulations and all-atom molecular dynamics simulations in implicit solvent) were applied to reveal the binding processes of ligands as they enter the binding site of the HIV-1 protease. The initial structures used for the molecular dynamics simulations were generated based on the Brownian dynamics trajectories, and this is the first molecular dynamics simulation of modeling the association of a ligand with the protease. We found that a protease substrate successfully binds to the protein when the flaps are fully open. Surprisingly, a smaller cyclic urea inhibitor (XK263) can reach the binding site when the flaps are not fully open. However, if the flaps are nearly closed, the inhibitor must rearrange or binding can fail because the inhibitor cannot attain proper conformations to enter the binding site. Both the peptide substrate and XK263 can also affect the protein's internal motion, which may help the flaps to open. Simulations allow us to efficiently study the ligand binding processes and may help those who study drug discovery to find optimal association pathways and to design those ligands with the best binding kinetics.

Key words: association rate, binding kinetics, drug design, gating effects

Received 29 November 2006, revised 13 December 2006, accepted for publication 19 December 2006

Binding two free molecules to form a complex is one of the most important processes in biological systems (e.g., a drug molecule binding to a protein, a substrate binding to an enzyme, or a protein binding to another protein). Binding plays roles in functions as diverse as metabolism, immunity, and signal transduction. For example, in human immunodeficiency virus type 1 (HIV-1), the viral polyprotein must bind to the active site of the HIV-1 protease to produce mature proteins to continue viral replication (1). The binding pathway has been proposed to occur when the two molecules diffuse together, then the specific contacts form. The first step may be driven by nonspecific and long-range electrostatic forces, whereas the second step may reflect more specific short-range interactions. The two steps may not be wholly separable, and the conformations of both molecules may change to adapt to each other and to form specific contacts when they come close to each other.

For two molecules approximated as uniformly reactive spheres, with no long-range interaction, the diffusion-limited association rate constant is roughly 10^9–10^{10} /(Msec). However, actual rate constants span a wide range of values, from 10^3 to 10^{10} /(Msec) for binding events of protein–ligand or protein–protein systems (2,3). This wide range reflects molecular and hydrodynamic interactions, geometric constraints of the binding sites, and variations in binding site accessibility as a result of protein internal motions (''gating'' effects) (4–14). If the association rate constant is mainly dominated by the diffusion process, the rate can be well modeled by Brownian dynamics simulations (15,16). However, for the more complicated two-step binding process, more detailed simulation techniques, as well as theoretical work, are necessary.

Although electrostatic effects have long been considered the most important element in altering the association rate constant (k_{on}), other factors are also key (e.g., binding site accessibility). In the case of HIV-1 protease, rate constants have been found in the range of 10^4–10^6 /(Msec) when the protease is binding a peptide substrate, but the range changes to 10^5–10^7 /(Msec) when the protease is binding a peptidomimic drug (17–20). The peptidomimic drugs are usually smaller than the experimentally used peptide substrate (~7 to 10 residues), and the drugs are neutral.

Interestingly, for another class of structurally different HIV-1 protease inhibitors, the cyclic urea inhibitors, the k_{on} can be ~10^9 to 10^{10} /(Msec), which is closer to the diffusion limit (21). Although these different classes of inhibitors have similar binding affinities, it is unclear why they display different kinetic features. The neutral cyclic urea inhibitors (e.g., inhibitor DMP323 and XK263) are also similar in size to peptidomimic drugs. However, they have been suggested having a high degree of preorganization, that is, the bound and unbound forms of cyclic urea inhibitor have similar conformations (22).

For the present study, we applied a recently developed coarse-grained model and the Brownian dynamics (BD) algorithm to simulate the binding of a peptide substrate or a cyclic urea inhibitor, XK263, to HIV-1 protease (8,23–25). The active site of the HIV-1protease is covered by two flaps that serve as a sort of 'gate', which needs to open for polyprotein binding. Although there is no 'wide open' HIV-1 protease crystal structure, NMR experiments for the free enzyme show substantial conformational fluctuations in the flap region (17,26). Consequently, using a coarse-grained force field not only allows to study the flap conformation but also provides a fast simulation method to study multiple ligand–protease binding pathways. We followed the binding pathways suggested by this model, then carried out a molecular dynamics simulation in an all-atom representation for the XK263-protease system.

Results from these simulations showed that the flaps must open to bind the linear peptide substrate, but a smaller XK263 inhibitor can bind into the active site while the gate is nearly closed. Unexpectedly, from our BD simulations, we observed that the intermolecular interactions between the peptide substrate and the HIV-1 protease may facilitate the opening of the flaps.

Methods

Coarse-grained model and force field

Coarse-grained models are used to represent HIV-1 protease (Figure 1A) and its ligands. For the peptide substrate and the protease, each residue is represented by one bead placed on the Cα carbon (27–33). The HIV-1 protease is a homo dimer, and we represent it as a single molecule in our simulations. For the inhibitor XK263, each benzene and naphthalene is represented by one bead, with another bead placed in the middle of the cyclic urea ring (Figure 1B). The effective radius of each bead is reported in Supplementary material (34). The beads are linked by virtual bonds, bond angles, and dihedral angles. A coarse-grained force field for HIV-1 protease, previously developed by Tozzini and McCammon (23,24), was extended to include the solvent effects, via screened electrostatics and BD, as well as intermolecular interactions. The force field has been implemented into the UHBD simulation package (35). The potential energy function is a sum of the following interactions:

$$U = U_{\text{bond}} + U_{\text{angle}} + U_{\text{dihe}} + U^{\text{intra}}_{\text{Morsebond}} + U^{\text{intra}}_{\text{vdw}} + U^{\text{inter}}_{\text{vdw}} + U_{\text{elec}} \quad (1)$$

The bond and dihedral interactions are harmonic, and the angle term is in the quartic form (Supplementary material). For non-bonded intramolecular interactions (two beads not connected by a virtual bond, virtual angle or virtual dihedral), either a pseudo-Morse bond $U^{\text{intra}}_{\text{Morsebond}}$ or an intramolecular van der Waals interaction $U^{\text{intra}}_{\text{vdw}}$ is applied. Both terms have the functional form of a Morse potential (see Supplementary material). For van der Waals interactions between two molecules, we use the following functional form:

$$U^{\text{inter}}_{\text{vdw}} = 0.5\left[\left(\frac{r_i + r_j}{r_{ij}}\right)^8 - 1.5\left(\frac{r_i + r_j}{r_{ij}}\right)^6\right] \quad (2)$$

where r_i and r_j are the effective radii of beads i and j, respectively. Unlike typical Lennard–Jones potential, the $U^{\text{inter}}_{\text{vdw}}$ function has a weaker repulsive force around the minimum, which allows some overlaps between two beads. A cutoff is set at 15 Å for intramolecular interactions, and there is no cutoff for intermolecular interactions. The Coulombic interaction between each pair of beads i and j is $U_{\text{elec}} = q_i q_j / \varepsilon r_{ij}$, where r_{ij} is the distance between beads i and j. The inhibitor XK263 is neutral, and the net charge of the protease and the peptide substrate is +4e and +1e, respectively. As we did not use a detailed solvent model, we employed a distance-dependent dielectric coefficient ($\varepsilon_{ij} = 4r_{ij}$) to avoid unrealistic in vacuo Coulombic interactions. Note that the reference structures used to generate the parameters were from crystallographic coordinates (see All-atom molecular dynamics simulations, PDB ID), and all parameters are listed in the Supplementary material.

Brownian dynamics

The BD simulation algorithm used here is reported in several original publications (8,36,37). In this algorithm, we solve the Langevin equation of motion in the overdamped limit, and the resulting equation gives a Brownian trajectory. All parameters and equations used in the BD simulations can be found in a previous publication (8). Multiple simulations were performed, and each simulation was initiated from a different ligand position, or had different random number seeds.

The coarse-grained model makes it possible to use large time steps in BD simulations, and this study used a 50 fs time step. However, the large time step sometimes causes unfavorable clashes between the ligand and the protease beads. To avoid this problem, we introduced an adaptive time-step method (37,38): If a resulting BD trajectory produces a dihedral or van der Waals energy larger than a predetermined threshold, the code splits this 50-fs time step into five 10-fs time steps to generate a more reasonable motion.

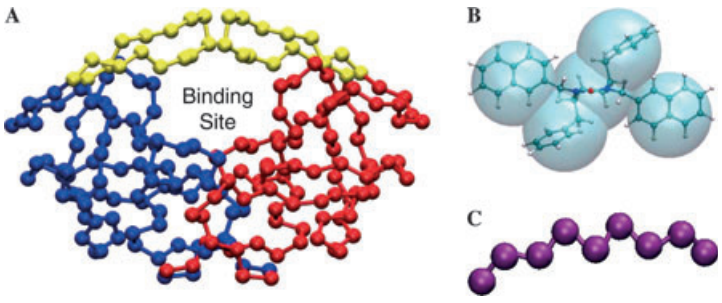

Figure 1: Coarse-grained representation. (A) HIV-1 protease. Blue: monomer A; red: monomer B; yellow: flaps (residues 43–55). (B) Inhibitor XK263. (C) Peptide substrate. The figure was prepared with VMD (49), and the sizes shown here do not reflect their actual sizes.

All-atom molecular dynamics simulations

Classical molecular dynamics simulations were performed using the AMBER package (39). The HIV-1 protease coordinates were obtained from the Protein Data Bank (PDB), ID 1HHP (40). The coordinates of peptide substrate and inhibitor XK263 were obtained from 1F7A and 1HVP, respectively (41,42). Hydrogen atoms were added by the LEAP module in AMBER, and all ionizable groups were assigned protonation states expected at pH 7. The FF99 molecular force field was used for the protein, and the ANTECHAMBER module and GAFF with AM1-BCC charges were used to obtain force field parameters for XK263 (43,44).

The generalized Born continuum solvent model was used to mimic the aqueous environment (45,46). The initial coordinates were subjected to a short energy minimization, and then gradually heated from 200 to 300 K. All production simulations were run at 300 K, and the temperature was maintained using Langevin dynamics with a collision frequency of 1 ps^{-1}. For the simulations, we used a 2-fs time step (see Results and Discussion for the duration of each simulation). All bonds involving hydrogen were constrained, and the cutoff was set to 40 Å when calculating non-bonded interactions.

Results and Discussion

We denote open and closed conformations of the protease based on the flap tip distance, which is defined by the distance between two flap tips (residue Ile50) from each monomer. If the tip distance is larger than 10 Å, the conformations are defined as open conformations; otherwise, they are closed. Moreover, we use the contact distance (d_{con}) to describe the position of the ligand relative to the protease. In our coarse-grained simulations, the contact distance is defined as the distance between the central bead of XK263 and the Asp25 bead in the protease monomer A. In the all-atom representation, d_{con} is defined as the distance between the XK263 center of mass and the center of mass of the protease excluding the flaps.

Overall binding processes

We studied the binding processes of the peptide substrate and inhibitor XK263 using BD trajectories. In the first step, we performed more than forty 2–5-μs BD simulations to explore possible association pathways of the inhibitor XK263 or the substrate when they formed a ligand–protein complex. The simulations revealed several distinct features of binding processes. During the simulations, the protease flaps can sample completely open and closed conformations when a ligand is not near its binding site. The protein dynamics are similar to results from previous studies on the apo form of the protease (8,24). The average lifetimes of the open and closed conformations were 70 and 430 ns, respectively. The opening fraction is in agreement with that previously obtained with the same set of bead radii and force field (8,24). Unlike the free protease, when the peptide substrate is in the active site but the flaps are still open, they always remain in this state much longer, taking on the order of 1 μs to close. Similarly, when the substrate is present in the active site with closed flaps, the flaps can remain closed longer than 1 μs. The substrate interacts with the protein, and thus alters the protease internal motion. The XK263-protease interactions were also observed to affect flap dynamics, but these effects are smaller than those found in the substrate–protease binding case.

Flap opening and substrate binding

It has been suggested that the protein flaps modulate binding-site accessibility and that they must open for segments of the polyprotein to bind. Once the appropriate region of the polyprotein is in the active site, the flaps close over the substrate, thereby allowing the enzyme to function (1). Our protein and substrate simulations showed that the gate must open to allow for the substrate binding. If the gate is closed when the substrate diffuses to the protease, the substrate may either diffuse away from the enzyme or stay for a while until the gate opens, and then bind to the active site. In the latter case, the substrate may form an interaction between one of the flaps that may cause asymmetric motion of the flaps, weakening the flap–flap tip attractions, and then facilitating the gate to open (Figure 2).

Figure 2 illustrates one simulation that has a successful binding. At 538.5 ns, while one flap was open, the other flap became more flexible, allowing the substrate access to the binding site. Once the substrate reached the binding site, it remained there until the flaps closed, which took from a few hundred nanoseconds to 1 μs. The molecules then stayed in the complex form for longer than 500 ns, until the simulation ended. Note that we only studied the wild-type protease. Different protease mutants may have different responses to the intermolecular interactions with the substrate.

XK263 binding pathways

Unlike the peptide substrate, the smaller inhibitor XK263 can bind from the top of the protease when the gate is open, or from the side when the gate is nearly closed, which was unexpected (Figures 3 and 4). From our simulations, since the flap opening fraction is only about 15% in the free protease, the most common XK263 binding pathways are from the side. However, the inhibitor XK263 binds to the protease easily when the flaps are open. In contrast, if binding from the side, it takes XK263 longer to explore the appropriate binding position during the diffusion processes. As shown in Figure 3, starting from a contact distance $d_{con} = 20$ Å, XK263 takes 1 ns to get to its final bound position when the flaps are open. When the flaps are semi-closed, XK263 needs 10 ns for complete binding. Note that this semi-closed structure falls in the closed class according to our classification, although in the literature, similar structures are often called ''semi-open''.

Although the binding site is easily accessible when the flaps are open, the flaps do need time to close and stabilize the complex conformation. Before the gate is closed, XK263 may leave the binding site, resulting in an unsuccessful binding. Figure 3B shows where the inhibitor tried to leave the binding site several times (e.g., near 4.5 and 15 ns) but it returned again. The flap finally closed at simulation time 25 ns. After that, the flaps prevented further escape attempts by the inhibitor. The final XK263 position in the bound state is very similar to the crystal structure for this complex, although, because of the coarse-grained representation, the

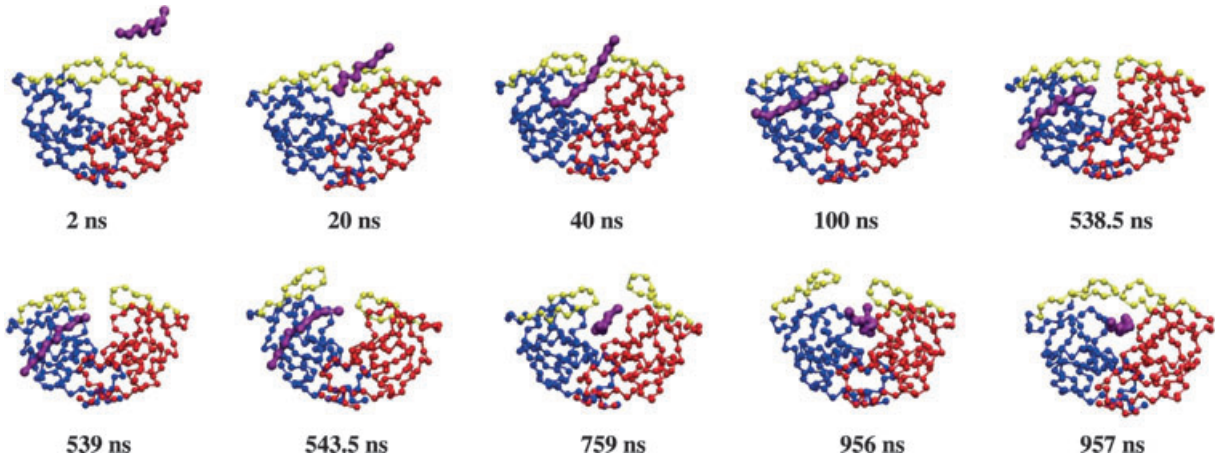

Figure 2: Transition of the peptide substrate from an unbound to a final bound state. The total simulation length in this run was 2 μs. The protein and the substrate are coarse-grained bead representation. Colors: blue - monomer A; red - monomer B; yellow - flaps; purple - the peptide substrate.

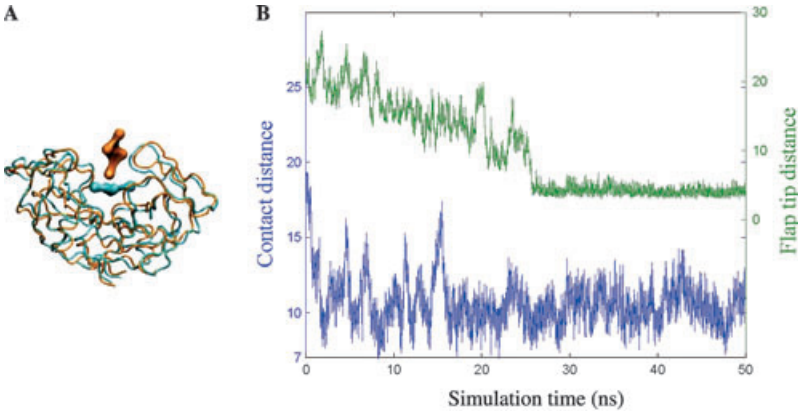

Figure 3: Coarse-grained BD simulation for the XK263-protease system. (A) XK263 binding to HIV-1 protease with open flaps. (B) Left *Y*-axis: contact distance (Å); right *Y*-axis: flap tip distance (Å); *X*-axis: simulation time. Orange: initial coordinate at simulation time 0 ns; Cyan: ligand bound state at 25 ns.

flaps do not adopt exactly the same conformation (figure not shown).

It is worth noting that because our coarse-grained models do not have detailed atomic interactions and explicit water molecules, the time scales exhibited here might not correspond exactly to experiments. Moreover, slightly different binding routes can be observed from different runs, but only three representative binding pathways are shown here.

We further analyzed XK263 association behavior with semi-closed gate conformations. Unlike the open flap protein conformation that allows various ligand binding orientations and directions, it is not possible for the ligand to access the binding site in an arbitrary way when the gate is semi-closed. Although previous publications suggest that the other very similar cyclic urea inhibitor, DMP232, has similar bound and unbound conformations (22), we found that XK263 could not reach the entrance if it always remained in the bound state conformation. As the inhibitor is represented by five beads in our coarse-grained model, it does not exhibit sidechain rotation of the benzene and naphthalene groups. Even though our simplified model cannot accurately represent the detailed side-chain interactions, it still can participate in less specific interactions, such as hydrophobic attractions and steric clashes. In Figure 4A–C, the molecule rearranged its orientations to fit the narrow entrance on one side of the protein. The inhibitor diffused, as well as rotated itself to get closer to the protein (Figure 4A, from silver to black ligand position). The XK263 orientation (Figure 4, black) was similar to its final bound state orientation (Figure 4C, cyan) but their positions were different. However, the inhibitor cannot always remain in this orientation, because the entrance to the active side is not wide enough for this conformation. The XK263 thus rotated again (Figure 4, red conformation), and it was gradually turning while approaching the bound state. As a result, the conformation adjustments require the ligand to spend more time getting into the final bound position, compared to the binding route shown in Figure 3.

It is also possible for XK263 to bind without altering its orientation when it diffuses near the active site. However, this only happens when the flaps are slightly more open than in a semi-closed conformation (Figure 5, loop region in red). Although this binding route seems straightforward, it is uncommon. The XK263-flap interactions may affect the flap conformation, thus facilitating flap opening. However, the details of such events are difficult to extract from

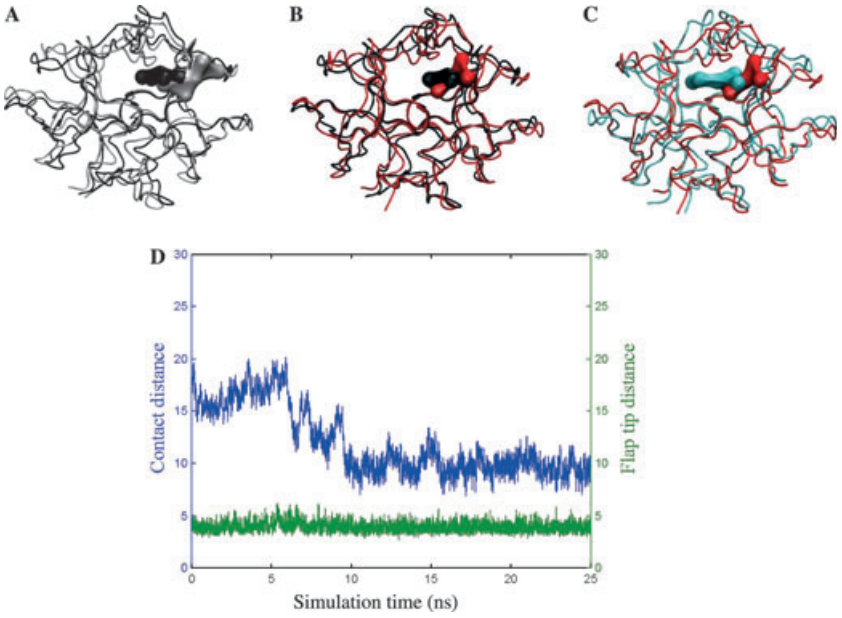

Figure 4: Coarse-grained BD simulation for the XK263-protease system. (A–C) XK263 binding to the HIV-1 protease with semi-closed flaps. (D) Left *Y*-axis: contact distance (Å); right *Y*-axis: flap tip distance (Å); *X*-axis: simulation time. Silver: outside the binding site at simulation time 5 ns; black: snapshot from 8 ns; red: snapshot from 9.3 ns; cyan: XK263 bound state at 10 ns (final bound state conformation).

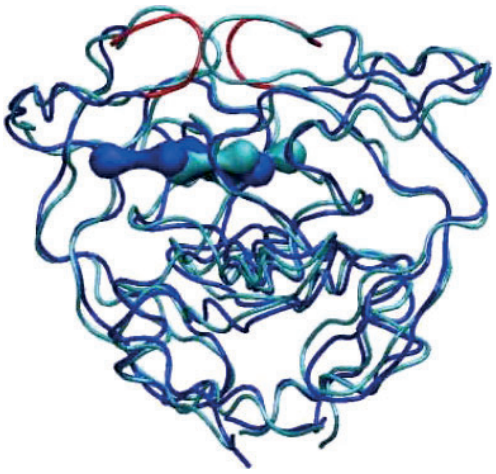

Figure 5: XK263 binding to the protease with partially open flaps. Blue: XK263 entering the binding site when flaps were partially open (flap tips shown in red); cyan: XK263 bound conformation.

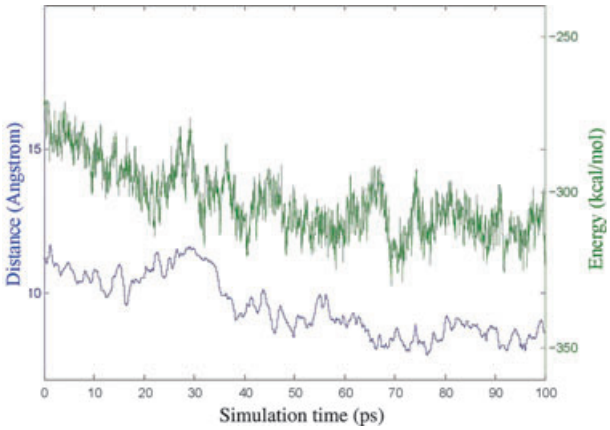

Figure 6: XK263-protease contact distance and their interaction energy during a molecular dynamics simulation. Left *Y*-axis: contact distance (Å). Right *Y*-axis: interaction energies between XK263 and the HIV-1 protease. *X*-axis: simulation time.

coarse-grained simulations. Unlike the nine beads peptide substrate that can be very flexible, the inhibitor has only five beads in a rigid shape. Therefore, XK263-protease interactions may not be sufficient enough to capture some features of flaps-XK263 interactions, as shown in Figure 2. Because of its smaller molecular size and pre-organization, XK263 seems to access the HIV-1 protease binding site easier than the peptide substrate. This may be one explanation for why the inhibitor has a faster association rate constant than the peptide substrate.

All-atom molecular dynamics simulations

To study detailed molecular interactions when XK263 binds to the semi-closed protease, and to confirm the pathways we learned from the coarse-grained modeling, two all-atom molecular dynamics simulations were performed. The first simulation was initiated from the conformation shown in Figure 4 (black), with XK263 remapped to its all-atom representation. The coarse-grained protein representation was replaced by the crystal structure (PDB code 1HHP) (40), as the backbone conformations are similar. Figure 6 shows that XK263 gradually moves toward the final bound state, which has a favorable potential energy. The contact distance was started at d_{con} ~11 Å, and the final position had d_{con}~7.5 Å.

In regards to the coarse-grained model, XK263 and the protease took time to rearrange their conformations. We observed the side-chain reorganization (Figure 7) where XK263 rotated both the naphthalene groups to form a more compact conformation for entering the protein (Figure 7, blue conformation). After some shifting in the binding site, both naphthalene side chains extended again, which

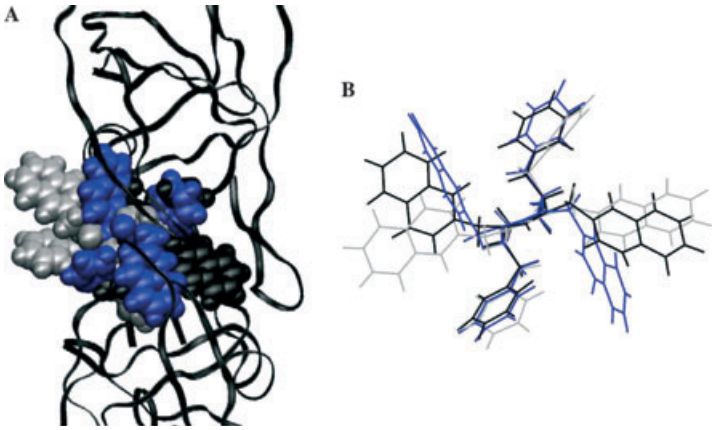

Figure 7: (A) XK263 binding pathways from a molecular dynamics simulation. Complex conformations were superimposed using the Bio3D package (50); only one protein conformation is shown. (B) XK263 conformations superimposed by cyclic urea. Silver: snapshot taken from simulation time 0 ps; blue: 10 ps; black: after 50 ps.

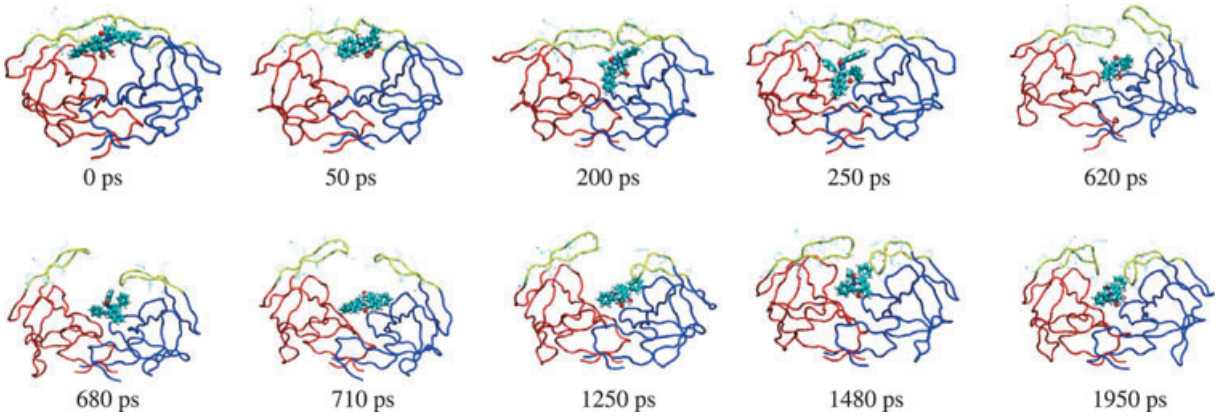

Figure 8: Transition of the inhibitor XK263 from an unbound to a final bound state. The total simulation length in this run was 2500 ps. The protein and XK263 are shown in tube and stick-ball representation, respectively. Flaps are shown in stick representation. Colors of the protease: blue - monomer A; red - monomer B; yellow - flaps.

allowed more contacts with the protein and the flaps somewhat, too. Note that the flaps did not open during this binding process.

The second molecular dynamics simulation was started from another BD snapshot (figure not shown), where the contact distance was around 17 Å. The inhibitor was again remapped to an all-atom representation, and the protease crystal structure from PDB 1HHP was used (Figure 8). Unlike the previous simulation where the inhibitor came closer to the center of the active site, here it came aside the flaps and interacted with the flap residues near the protein surface. When XK263 shifted toward the binding site, the flaps also moved slightly inward, perhaps due to XK263-flap interactions. The intermolecular interactions again caused an asymmetric motion of the flaps (620 ps), with one flap curled down to allow a partially open flap orientation (680 ps). The inhibitor then smoothly moved to the bound position (710 ps). The flaps continued to fluctuate significantly for several hundred picoseconds, until they formed more stable interactions with the inhibitor (1480 ps). The flaps curled down to interact with XK263, but they did not reach the final closed form seen in the crystal structure in this 2500 ps simulation. The XK263-protease interaction energies fluctuated even after the inhibitor remained close to its bound position in the bottom of the active site (Figure 9). As we have seen in coarse-grained simulations, the ligand–protease interactions may influence the protein dynamics, thus opening a flap and facilitating ligand binding. Moreover, one can envision that different protease mutants may have

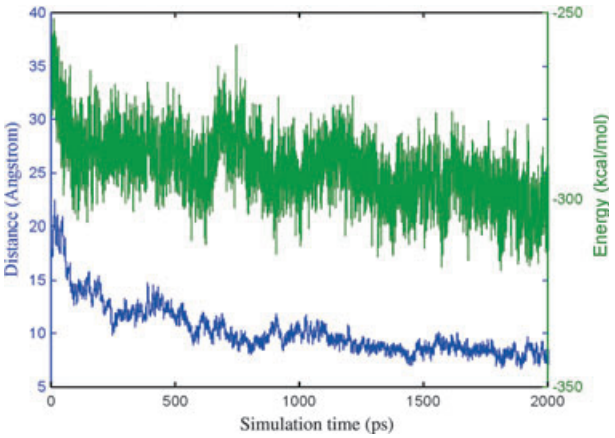

Figure 9: XK263-protease contact distance and their interaction energy during a molecular dynamics simulation. Left *Y*-axis: contact distance (Å). Right *Y*-axis: interaction energies between XK263 and the HIV-1 protease. *X*-axis: simulation time.

different dynamic changes because of the ligand–protein interactions, as protein rigidity varies with mutations.

In summary, the first molecular dynamics simulation suggests that with proper conformations, XK263 can enter the binding site without opening the flaps. This is in good agreement with our coarse-grained BD simulations. The second molecular dynamics simulation shows another possible binding pathway, in which XK263 can induce partial flap opening and bind to the protease with the flaps not fully open. The change in the flap conformation due to the intermolecular interactions was not observed in the XK263-protease BD simulations, perhaps due to the coarse-grained force field. Nevertheless, we did see similar flap motions in the substrate–protease BD runs.

Conclusions

The present work applies the multiscale simulation methods to study ligand–HIV-1 protease binding pathways. First, fast coarse-grained BD simulations were carried out, followed by all-atom molecular dynamics simulations which were performed using the results of the coarse-grained simulations as a guide to generate the initial structures. This study shows that there are several possible binding processes involved. The peptide substrate can only access the HIV-1 protease binding site when the flaps are open. The substrate may induce asymmetric flap motions, which may facilitate the flap opening. In contrast, the inhibitor XK263 binds to the protease when the flaps are open or semi-closed, but a proper XK263 orientation is necessary for it to access the binding site. The association rate constants (k_{on}) are in the range of 10^4–10^6 and 10^9–10^{10} /(Msec), respectively, when the protease is binding a peptide substrate or a cyclic urea inhibitor (17,19). The conformation of XK263 makes it easier to access the binding site of the protease, which may explain why it displays fast kinetic features. The results highlight the potential to gain affinity by designing conformationally preferable ligands to reach fast k_{on}. Our coarse-grained simulations also showed that after the ligand moved to the active site of the protease, the substrate–open protease complex needed more time for the flaps to close, compared to the XK263-open protease complex. This observation is consistent with results from recent all-atom molecular dynamics simulations (47,48). The final bound states of both XK263 and the peptide substrate were close to the crystal structure of the bound complex. Our all-atom molecular dynamics study again shows that the size and conformation of XK263 allow it to enter the active site when the flaps are semi-closed. Moreover, the molecular dynamics runs carried out for XK263-protease showed that intermolecular interactions may facilitate flap opening, which we observed in the substrate–protease BD runs.

Acknowledgments

CC thanks Drs Rommie Amaro and Xiaolin Cheng for discussions. This work was supported in part by NIH, NSF, the Howard Hughes Medical Institute, the National Biomedical Computational Resource, the NSF Center for Theoretical Biological Physics, the W. M. Keck Foundation and Accelrys, Inc. JT was supported by the Warsaw University funds (115/30/E-343/S/BST-1140/ICM/2006) and by Polish Ministry of Science and Higher Education (3 T11F 005 30, 2006–2008).

References

1. Libman H., Makadon H.J. (2003) HIV. Philadelphia: American College of Physicians.
2. Song Y., Zhang Y., Shen T., Bajaj C.L., McCammon J.A., Baker N.A. (2004) Finite element solution of the steady-state Smoluchowski equation for rate constant calculations. Biophys J;86:2017–2029.
3. Schreiber G. (2002) Kinetic studies of protein–protein interactions. Curr Opin Struct Biol;12:41–47.
4. Northrup S.H., Erickson H.P. (1992) Kinetics of protein–protein association explained by Brownian dynamics computer simulation. Proc Natl Acad Sci USA;89:3338–3342.
5. Shaul Y., Schreiber G. (2005) Exploring the charge space of protein–protein association: a proteomic study. Proteins: Structure, Function Bioinformatics;60:341–352.
6. Schlosshauer M., Baker D. (2002) A general expression for bimolecular association rates with orientational constraints. J Phys Chem B;106:12079–12083.
7. Das A., Jayaram B. (1998) Brownian dynamics simulations of DNB-ligand interactions: A theoretical study on the kinetics of DAPI-DNA complexation. J Mol Liquids;77:157–163.
8. Chang C.E., Shen T., Trylska J., Tozzini V., McCammon J.A. (2006) Gated binding of ligands to HIV-1 protease: Brownian dynamics simulations in a coarse-grained model. Biophys J;90:3880–3885.
9. Edmondson D.E., Mattevi A., Binda C., Li M., Hubalek F. (2004) Structure and mechanism of monoamine oxidase. Curr Med Chem;11:1983–1993.
10. Ahvazi B., Boeshans K.M., Rastinejad F. (2004) The emerging structural understanding of transglutaminase 3. J Struct Biol;147:200–207.
11. Hucho F., Tsetlin V.I., Machold J. (1996) The emerging three-dimensional structure of a receptor – The nicotinic acetylcholine receptor. Eur J Biochem;239:539–557.
12. McCammon J.A., Northrup S.H. (1981) Gated binding of ligands to proteins. Nature;151:316–317.
13. Szabo A., Shoup D., Northrup S.H., McCammon J.A. (1982) Stochastically gated diffusion-influenced reactions. J Chem Phys;77:4484–4493.
14. Mihailescu M., Gilson M.K. (2004) On the theory of noncovalent binding. Biophys J;87:23–36.
15. Wade W.C., David M., Luty B.A., Madura J.D.E.M., McCammon J.A. (1993) Ating of the active-site of triose phosphate isomerase - brownian dynamics simulations of flexible peptide loops in the enzyme. Biophys J;64:9–15.
16. Spaar A., Dammer C., Gabdoulline R.R., Wade R.C., Helms V. (2006) Diffusional encounter of barnase and barstar. Biophys J;90:1913–1924.

17. Katoh E., Louis J.M., Yamazaki T., Gronenborn A.M., Torchia D.A., Ishima R. (2003) A solution NMR study of the binding kinetics and the internal dynamics of an HIV-1 protease–substrate complex. Protein Sci;12:1376–1385.
18. Szeltner Z., Polgar L. (1996) Rate-determining steps in HIV-1 protease catalysis - The hydrolysis of the most specific substrate. J Biol Chem;271:32180–32184.
19. Shumana C.F., Markgren P.-O., Hamalainen M., Danielson U.H. (2003) Elucidation of HIV-1 protease resistance by characterization of interaction kinetics between inhibitors and enzyme variants. Antiviral Res;58:235–242.
20. Maschera B., Darby G., Palu G., Wright L.L., Tisdale M., Myers R., Blair E.D., Furfine E.S. (1996) Human immunodeficiency virus: Mutations in the viral protease that confer resistance to saquinavir increase the dissociation rate constant of the protease–saquinavir complex. J Biol Chem;271:33231–33235.
21. Markgren P.-O., Schaal W., Haaanen M., Karle A., Hallberg A., Samuelsson B., Danielson U.H. (2002) Relationships between structure and interaction kinetics for HIV-1 protease inhibitors. J Med Chem;45:5430–5439.
22. Lam P.Y.S., Ru Y., Jadhav P.K., Aldrich P.E., DeLucca G.V., Eyermann C.J., Chang C.-H. et al. (1996) Cyclic HIV protease inhibitors: Synthesis, conformational analysis, P2/P2F structure-activity relationship, and molecular recognition of cyclic ureas. J Med Chem;39:3514–3525.
23. Tozzini V., McCammon J.A. (2005) A coarse grained model for the dynamics of flap opening in HIV-1 protease. Chem Phys Lett;413:123–128.
24. Tozzini V., Trylska J., Chang C.E., McCammon J.A. (2007) Flap opening dynamics in HIV-1 protease explored with a coarse-grained model. J Struct Biol; in press.
25. Minh D.D.L., Chang C.E., Trylska J., Tozzini V., McCammon J.A. (2006) the influence of macromolecular crowding on HIV-1 protease internal dynamics. J Am Chem Soc;128:6006–6007.
26. Freedberg D.I., Ishima R., Jacob J., Wang Y.X., Kustanovich I., Louis J.M., Torchia D.A. (2002) Rapid structural fluctuations of the free HIV protease flaps in solution: Relationship to crystal structures and comparison with predictions of dynamics calculations. Prot Sci;11:221–232.
27. Muller-Plathe F. (2002) Coarse-graining in polymer simulation: From the atomistic to the mesoscopic scale and back. Chemphyschem;3:754–769.
28. McCammon J.A., Northrup S.H. (1980) Helix-coil transitions in a simple polypeptide model. Biopolymers;19:2033–2045.
29. Reith R., Meyer H., Muller-Plathe F. (2001) Mapping atomistic to coarse-grained polymer models using automatic simplex optimization to fit structural properties. Macromolecules;34:2335–2345.
30. Tozzini V. (2005) Coarse-grained models for proteins. Curr Opin Struct Biol;15:144–150.
31. Trylska J., Tozzini V., McCammon J.A. (2005) Exploring global motions and correlations in the ribosome. Biophys J;89:1455–1463.
32. Karanicolas J., Brooks C.L. (2002) The origins of asymmetry in the folding transition states of protein L and protein G. Prot Sci;11:2351–2361.
33. Veitshans T., Klimov D., Thirumalai D. (1996) Protein folding kinetics: Timescales, pathways and energy landscapes in terms of sequence-dependent properties. Folding Des;2:1–22.
34. Reva B.A., Finkelstein A.V., Sanner M.F., Olson A.J. (1997) Residue-residue mean-force potentials for protein structure recognition. Prot Eng;10:865–876.
35. Davis M.E., Madura J.D., Luty B.A., McCammon J.A. (1991) Electrostatics and diffusion of molecules in solution: Simulations with the University of Houston Brownian Dynamics Program. Comput Phys Commun;62:187–197.
36. Ermak D.L., McCammon J.A. (1978) Brownian dynamics with hydrodynamic interactions. J Chem Phys;69:1352–1360.
37. Shen T.Y., Wong C.F., McCammon J.A. (2001) Atomistic Brownian dynamics simulation of peptide phosphorylation. J Am Chem Soc;123:9107–9111.
38. Press W.H., Flannery B.P., Teukolsky S.A., Vetterling W.T. (1989) Numerical Recipes. The Art of Scientific Computing. Cambridge: Cambridge University Press.
39. Case D.A., Cheatham T.E., Darden T., Gohlke H., Luo R., Merz K.M., Onufriev A., Simmerling C., Wang B., Woods R.J. (2005) The Amber biomolecular simulation programs. J Comput Chem;26:1668–1688.
40. Spinelli S., Liu Q.Z., Alzari P.M., Hirel P.H., Poljak R.J. (1991) The three-dimensional structure of the aspartyl protease from the HIV-1 isolate BRU. Biochimie;73:1391–1396.
41. Prabu-Jeyabalan M., Nalivaika E., Schiffer C.A. (2000) How does a symmetric dimer recognize an asymmetric substrate? A substrate complex of HIV-1 protease. J Mol Biol;301:1207–1220.
42. Lam P.Y., Jadhav P.K., Eyermann C.J., Hodge C.N., Ru Y., Bacheler L.T., Meek J.L., Otto M.J., Rayner M.M., et al. (1994) Y. N. W. Rational design of potent, bioavailable, nonpeptide cyclic ureas as HIV protease inhibitors. Science;263:380–384.
43. Cornell W.D., Cieplak P., Bayly C.I., Gould I.R., Merz K.M., Ferguson D.M., Spellmeyer D.C., Fox T., Caldwell J.W., Kollman P.A. (1995) A second generation force field for the simulation of proteins, nucleic acids, and organic molecules. J Am Chem Soc;117:5179–5197.
44. Wang J., Wolf R.M., Caldwell J.W., Kollman P.A., Case D.A. (2004) Development and testing of a general amber force field. J Comput Chem;25:1157–1174.
45. Onufriev A., Bashford D., Case D.A. (2004) Exploring protein native states and large-scale conformational changes with a modified generalized born model. Proteins: Structure, Function, and Bioinformatics;55:383–394.
46. Still W.C., Tempczyk A., Hawley R.C., Hendrickson T. (1990) Semianalytical treatment of solvation for molecular mechanics and dynamics. J Am Chem Soc;112:6127–6129.
47. Hornak V., Okur A., Rizzo R.C., Simmerling C. (2006) HIV-1 protease flaps spontaneously close to the correct structure in simulations following manual placement of an inhibitor into the open state. J Am Chem Soc;128:2812–2813.
48. Toth G., Borics A. (2006) Closing of the flaps of HIV-1 protease induced by substrate binding: A model of a flap closing mechanism in retroviral aspartic proteases. Biochemistry;45:6606–6614.
49. Humphrey W., Dalke A., Schulten K. (1996) VMD -visual molecular dynamics. J Mol Graph;14:33–38.
50. Grant B., Rodrigues A., ElSawy K.M., McCammon J.A., Caves L. (2006) Bio3D: An R package for the comparative analysis of protein structures. Bioinformatics; 22:2695–2696.

Supplementary Material

The following supplementary material is available for this article:

Appendix S1. This material includes the equations and parameters used in the coarse-grained force field, effective radii for the protein, peptide and XK263, an example of potential energy for angle term (Figure 1), and equilibrium value of angles for each amino acid (Table 1).

This material is available as part of the online article from: http://www.blackwell-synergy.com/doi/abs/10.1111/j.1747-0285.2007.00464.x (This link will take you to the article abstract).

Please note: Blackwell Publishing are not responsible for the content or functionality of any supplementary materials supplied by the authors. Any queries (other than missing material) should be directed to the corresponding author for the article.